Heliyon 10 (2024) e32232

Contents lists available at ScienceDirect

Heliyon

journal homepage: www.cell.com/heliyon

Research article

Optical coherence tomography-derived texture-based radiomics features identify eyes with intraocular inflammation in the HAWK clinical trial

Sudeshna Sil Kar [a], Hasan Cetin [b], Sunil K. Srivastava [b,d], Anant Madabhushi [a,c,**,1], Justis P. Ehlers [b,d,*,1]

[a] Department of Biomedical Engineering, Emory University, Atlanta, GA, USA
[b] The Tony and Leona Campane Center for Excellence in Image-Guided Surgery and Advanced Imaging Research, Cole Eye Institute, Cleveland Clinic, Cleveland, OH, USA
[c] Atlanta Veterans Administration Medical Center, Atlanta, GA, USA
[d] Vitreoretinal Service, Cole Eye Institute, Cleveland Clinic, Cleveland, OH, USA

ARTICLE INFO

Keywords:
Intraocular inflammation
Radiomics
Optical coherence tomography
Neovascular age-related macular degeneration
Vascular endothelial growth factor

ABSTRACT

Background and objective: Intravitreal injection of anti-VEGF agents is the first-line treatment for patients with neovascular-age related macular degeneration (nAMD). One unique serious adverse event that may be associated with these agents is intraocular inflammation (IOI). The main purpose of this analysis was to evaluate the potential presence of texture-based radiomics features characterizing heterogeneity within the vitreous compartment of spectral domain optical coherence tomography (SD-OCT) images that may precede or develop in association with IOI and might serve as OCT biomarkers for IOI.

Methods: This is a post-hoc analysis of a subset of cases (N = 67) involving IOI, endophthalmitis, and/or retinal vascular occlusion in the phase 3 HAWK trial. These were investigator determined diagnoses that were also confirmed by the safety review committee. Intraocular inflammation was any signs of inflammation within the eye, endophthalmitis was inflammation associated with presumed infection, and retinal vascular occlusions consisted of intraocular inflammation with concurrent vascular occlusions/vasculitis. Out of 67 eyes, 34 belonged to the Safety group with an IOI event and 33 were propensity-matched Controls. A total of 481 texture-based radiomics features were extracted from the vitreous compartment of the SD-OCT scans at pre-IOI time point (i.e., much earlier than the actual event). Most discriminating five features, selected by the Wilcoxon Rank Sum feature selection were evaluated using Random Forest (RF) classifier on the training set (S_{tr}, N = 47) to differentiate between the two patient groups. Classifier performance was subsequently validated on the independent test set (S_t, N = 20). Additionally, the classifier performance in discriminating the Control and Safety group was also validated on S_t at the IOI event timepoint.

Abbreviations: Intraocular Inflammation, (IOI); Optical Coherence Tomography, (OCT); neovascular Age-related Macular Degeneration, (nAMD); Vascular endothelial growth factor, (VEGF).

* Corresponding author. Cole Eye Institute, Cleveland Clinic, 9500 Euclid Avenue/Desk i32, Cleveland, OH 44195, USA.
** Corresponding author. Wallace H Coulter Department of Biomedical Engineering, Emory University and Georgia Institute of Technology, Research Career Scientist, Atlanta VA Medical Center, 1750 Haygood Drive, Suite 647, Atlanta, 30322, Georgia.
E-mail addresses: anantm@emory.edu (A. Madabhushi), ehlersj@ccf.org (J.P. Ehlers).
[1] Co-senior and Co-corresponding Authors.

https://doi.org/10.1016/j.heliyon.2024.e32232
Received 1 January 2024; Received in revised form 29 May 2024; Accepted 30 May 2024
Available online 13 June 2024

Results: The RF classifier yielded area under the Receiver Operating Characteristics curve (AUC) of 0.76 and 0.81 on S_t using texture-based radiomics features at pre-IOI and event time-point, respectively.
Conclusions: In this analysis, the presence of a pre-IOI safety signal was detected in the form of textural heterogeneity within the vitreous compartment even prior to the actual event being identified by the investigator. This finding may help the clinicians to assess for underlying posterior inflammation.

1. Introduction

Neovascular age-related macular degeneration (nAMD), the advanced form of macular degeneration, is characterized by the growth of choroidal neovascularization that originate from the choroid and breaks through the sub-retinal pigment epithelium (sub-RPE) space [1]. Vascular endothelial growth factor (VEGF) has been identified as the primary mediator involved in the pathogenesis of nAMD with higher expression of VEGF reported in the RPE and pre-Inner Limiting Membrane (pre-ILM)/vitreous of the retina [2]. Intravitreal injections through the inhibition of anti-VEGF agents such as aflibercept (Eylea; Regeneron), ranibizumab (Lucentis; Genentech), and bevacizumab (Avastin; Genentech) are currently the first-line standard for treatment of nAMD patients [3]. These agents inhibit the growth of abnormal blood vessels and have demonstrated their efficacy with superior anatomic outcome by substantial reduction in intra-retinal fluid (IRF), sub-retinal fluid (SRF), central subfield thickness (CST) [4]. For the vast majority of patients these therapeutics are very well tolerated with minimal side effect profile [5–7], however, a very small percentage of patients develop intraocular inflammation (IOI), one of the rare but major adverse events associated with these drugs [3]. The inflammation can result in the development of cellular debris within the vitreous compartment, the presence of which can lead to the formation of floaters, which are small specks or threads that appear to float in front of the eye. The inflammation can also lead to more serious complications, such as retinal vasculitis or macular edema. Developing computational imaging biomarkers (CIBs) characterizing the potential presence of IOI signals that may precede or develop in association with IOI could be an important tool to identify eyes that are at highest risk for developing IOI-related events and potentially prevent the clinicians to administer subsequent anti-VEGF injections that could result in a more severe IOI event.

Spectral-domain optical coherence tomography (SD-OCT) is the gold standard imaging modality for the management of nAMD and provides 3-dimensional (3D) imaging of intra-ocular tissue structures and retinal anatomy at micron resolution in a non-invasive way [8]. The unique phenotypic capabilities of OCT have triggered the development of multiple analytic platforms that can provide better understanding of ophthalmologic disease pathophysiology and differential therapeutic response. Radiomics-based characterization of SD-OCT images is an emerging field in ophthalmology and provides novel interpretable ways of identifying sub-visual patterns, features representing disease characteristics beyond human perception capacity [9]. Our group has been thoroughly investigating the role of SD-OCT derived biomarkers in predicting anti-VEGF therapy treatment response for diabetic macular edema (DME), retinal vein occlusion (RVO) and nAMD patients [10,11]. In a recent study, we have identified that the texture-based radiomics features characterizing heterogeneity within the texture of fluid and retinal tissue compartments were associated to anti-VEGF therapy treatment response prediction for DME and RVO [10]. We also performed longitudinal assessment of alterations in different texture-based radiomics descriptors between baseline and post-treatment SD-OCT scans (delta-texture features) for nAMD patients and found that the delta-texture features within sub-retinal hyper-reflective material (SHRM) were found to be most implicated in predicting therapeutic response [11].

In terms of IOI assessment, the published literature focuses on the association between the different characteristic features of IOI events and visual acuity (VA) loss [12], severity measurement and outcomes of IOI events [13], analysis of risk factors [14] and pathogenic contribution of inflammation in AMD [15]. These studies provide useful insights on the pathogenesis and adverse effects of inflammation, however, there is an unmet clinical need to identify the eyes who are likely to develop inflammation in the future. This could help the clinicians for future risk stratification of anti-VEGF drugs and prevent subsequent doses of anti-VEGF injection that could result in a more severe IOI response. OCT-based assessment of IOI may be characterized by vitreous cell/debris and potentially preretinal hyperreflective foci (PHF) within the vitreous compartment (i.e., pre-ILM) of SD-OCT scans. In the present study, we hypothesized that substantial variation within the texture of the vitreous compartment may exist between the patients who developed inflammation and who did not (i.e., Controls) due to the presence of hyperreflective deposits and PHF; radiomics-based characterization of the vitreous compartment may provide early signals of adverse events and more granular insight into the effect of anti-VEGF drugs.

With this aim in mind, we extracted different texture-based radiomics features characterizing heterogeneity within the pre-ILM/vitreous compartment from SD-OCT scans at pre-IOI event timepoint. The most discriminating features were selected using feature selection and used to train a Random Forest (RF) classifier on the training set (S_{tr}) to discriminate between the IOI and Control group and classifier performance was subsequently validated on the test set (S_t).

2. Methods

2.1. Study description and patient selection

HAWK [16] was a double-masked, multicenter, active controlled randomized phase 3 trial that compared the efficacy of aflibercept and brolucizumab in treating nAMD. The principles of the Declaration of Helsinki, International Conference on Harmonization E6 Good Clinical Practice Consolidated Guideline, and other regulations as required were followed to conduct the study. The study was also compliant with the Health Insurance Portability and Accountability Act of 1996. Written informed consent from all the patients were collected prior to screening or any study related procedure started. Macular cube scans focusing the foveal center point were obtained at each visit using SD-OCT, either with a Spectralis (Heidelberg) or Cirrus (Zeiss) system.

As part of post hoc review of clinical data [17], an independent Safety Review Committee (SRC), supported by Novartis Pharma AG, images were reviewed frame by frame for specific features prior to or during the IOI event. The SRC reviewed data from cases of investigator-reported IOI (30/1088 brolucizumab-treated eyes; 4/729 aflibercept-treated eyes) from the HAWK study and analyzed the presence of safety signal in their respective OCT scans and identified investigator-reported cases of IOI, retinal arterial occlusion and endophthalmitis. These were investigator determined diagnoses that were also confirmed by the safety review committee. Intraocular inflammation was any signs of inflammation within the eye, endophthalmitis was inflammation associated with presumed infection, and retinal vascular occlusions consisted of intraocular inflammation with concurrent vascular occlusions/vasculitis. In addition to the SRC identified IOI eyes, 34 eyes were identified as propensity-matched Controls. At the same time, the subject self-reported an adverse event of "vitreous floaters" that was logged as part of the study. Given the reported adverse event and the SD-OCT findings, this was determined to likely be an undetected IOI episode and this subject was excluded as a Control. One eye out of 34 Controls (3 %) demonstrated PHF and vitreous debris on OCT scans and was excluded from the present study.

The Cole Eye Institute, Cleveland Clinic performed an initial qualitative OCT inspection, 20 out of 34 eyes from the IOI group (59 %) demonstrated PHF and/or vitreous debris (11 eyes with PHF and/or vitreous debris at event time-point and 9 eyes with PHF and/or vitreous debris at prior-to-event time-point). The rest 14 eyes (41 %) did not have PHF and/or vitreous debris. Eight of these 14 eyes developed the most severe IOI-related adverse events: retinal vasculitis (RV) and retinal vascular occlusion (RO). The initial comparative qualitative assessment of the eyes used in the study is presented in Fig. 1.

2.2. Segmentation of vitreous compartment

The Cole Eye Institute, Cleveland Clinic performed a post hoc analysis of the OCT scans to segment fluid, retinal layers (Inner Limiting Membrane [ILM], Bruch's Membrane [BM], Retinal Pigment Epithelium [RPE]) using a proprietary multilayer segmentation

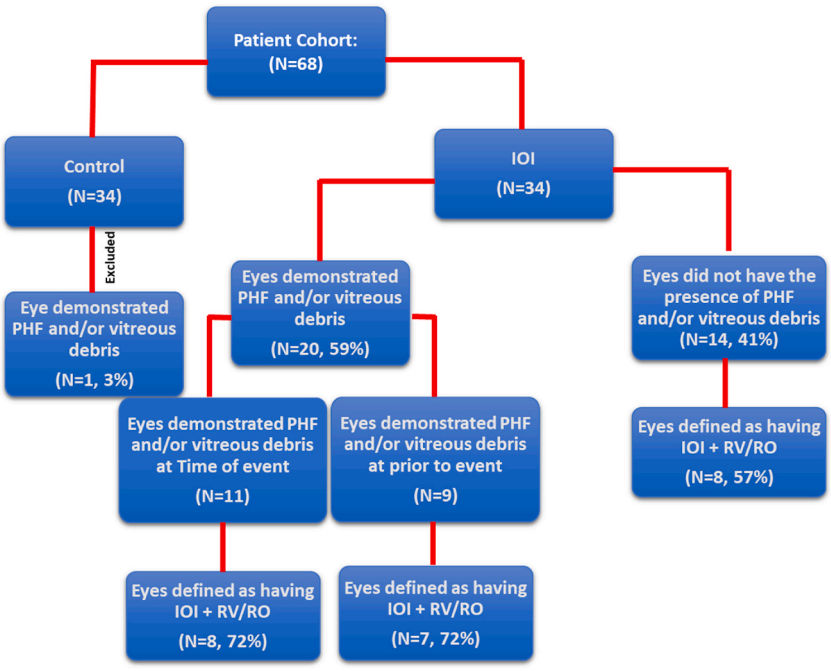

Fig. 1. Initial Comparative Qualitative Assessment of the Study Eyes: SRC performed an independent unmasked post hoc review of all cases of investigator-reported IOI, retinal vascular occlusions and endophthalmitis in the phase 3 HAWK study. 34 eyes were identified to have IOI by the SRC. SRC, Safety Review Committee; IOI, intraocular inflammation; OCT, optical coherence tomography; PHF, preretinal hyperreflective foci; RV, retinal vasculitis; RO, retinal vascular occlusion.

software/tool (developed by Cleveland Clinic) [18]. The pre-ILM region was segmented as vitreous compartment. The software/tool implemented image processing, machine learning (ML), and logic in an integrated platform for the segmentation followed by review of the segmentation lines by trained experts. The expert readers ensured segmentation accuracy by correcting the segmentation lines in standardized reading environment. For any given eye, all time points were evaluated by the same human reader. This other way ensured minimal inter-reader and inter-timepoint variability. Finally, the scans were evaluated by the experienced senior analyst for consistency and segmentation accuracy [17–19].

2.3. Radiomics feature extraction

We defined the sub-volumes corresponding to the vitreous compartment segmentation as I_v from the image I. From every voxel within $c_v \in \{I_v\}$, a set of 481 3-dimensional (3D) texture-based radiomics features (F_t) were extracted. The features within F_t belonged to the Haralick [20], Laws [21], Gabor [22] and CoLlage [23] feature family based on our previous work [10,11] demonstrating their promise in predicting therapeutic response for DME, RVO and nAMD patients. The detailed description of F_t is summarized in Supplemental Section I. For each feature within F_t, statistics of median, variance, skewness, and kurtosis were computed from the feature responses of all voxels within the region of interest and a total of 1924 statistical features were obtained. All the feature values were normalized with a zero mean and a standard deviation of one. Spearman's rank correlation test [24] that is robust to outliers and quantifies monotonicity was performed to compute Spearman correlation co-efficient (SCC) and the associated p-value for each pair of features. For any feature pair with SCC>0.8, the feature with higher p-value was pruned to eliminate redundant features. To control for the false discovery rate (FDR), the Benjamini and Hochberg method [25] was used to adjust the p values and features with p-value<0.05 was considered to be statistically significant.

2.4. Statistical analysis

The entire cohort of 67 patients was randomly divided into a training set (S_{tr}, N = 47) and a test set (S_t, N = 20) ensuring balance in the number of Controls and Safety patients within each set. S_{tr} comprised of 23 Controls and 24 patients from Safety group and S_t

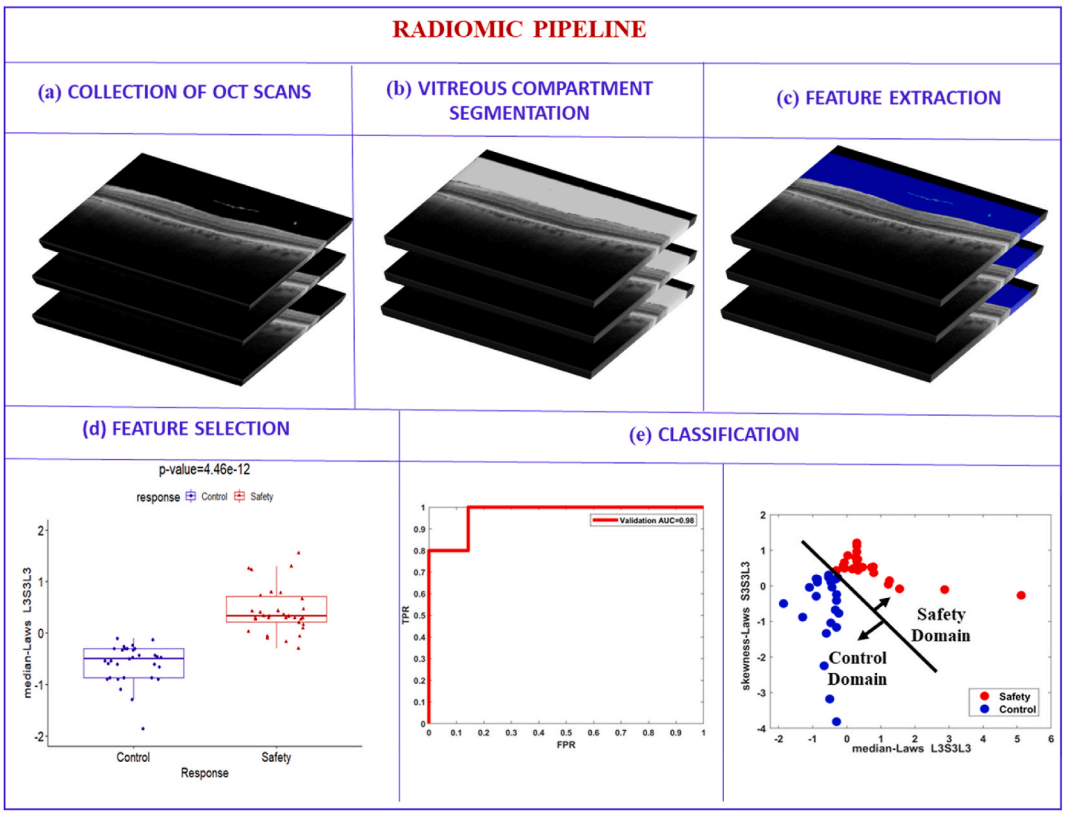

Fig. 2. Diagram of the Overall Radiomic Pipeline. *(a) SD-OCT scans were retrospectively collected. (b)Segmentation of pre-ILM/vitreous compartment using an ML based multi-layer segmentation platform OCTViewer. (c) Texture-based radiomic feature extraction (d) Wilcoxon-Rank Sum feature selection was used to select the top five features to train a RF classifier on S_{tr} (N=47). (e) Classifier performance (in terms of AUC) was validated on 20 patients in S_v. 2D scatter plot between the topmost two features show clear separation between the two groups of patients. SD-OCT, Spectral Domain-Optical Coherence Tomography; ILM, Inner Limiting Membrane; ML, Machine Learning, RF, Random Forest; AUC; Area under Receiver Operating Characteristics Curve.*

included 10 Controls and 10 patients from Safety group.

In the present study, to determine the features within F_t that best discriminated between the Control and Safety group at pre-IOI timepoint, the most discriminating set of radiomic features were selected from F_t by the Wilcoxon Rank Sum feature selection method. To reduce the likelihood of over-fitting the predictive model to S_{tr}, the top five (roughly one tenth of the number of samples) most frequently selected features from one thousand repetitions of three-fold cross-validation (CV) were identified based on voting across all repetitions of CV. In each repetition of CV, classification performance of the selected features was quantified using a RF classifier on S_{tr}. The RF model (M_{rf}) performance was subsequently validated on S_t using the area under receiver operating curve (AUC) metric. The other performance metrics included accuracy (ACC), sensitivity and specificity. Similarly, we evaluated the performance of M_{rf} on S_t to distinguish the two groups of patients at event timepoint.

To further investigate the generalizability of the developed radiomic model, we also evaluated the performance of M_{rf} in discriminating Control group from the more adverse event group with RV/RO at both the pre-IOI and event timepoints. Fig. 2 (a-e) shows the overall radiomic pipeline comprising radiomic feature extraction, feature selection followed by classification and validation.

3. Results

3.1. Patient characteristics

Based on the absence/presence of an inflammatory safety signal within the Phase III HAWK clinical trial, patients were categorized as Control (N = 34) and Safety (N = 34). One patient in the Control group was excluded due to presence of PHF and/or vitreous debris on OCT scans.

3.2. Distinguishing Control and Safety group based on texture-based radiomic features at pre-IOI and event timepoint

The most discriminating texture-based radiomic features that favorably distinguished between Control and Safety group of patients

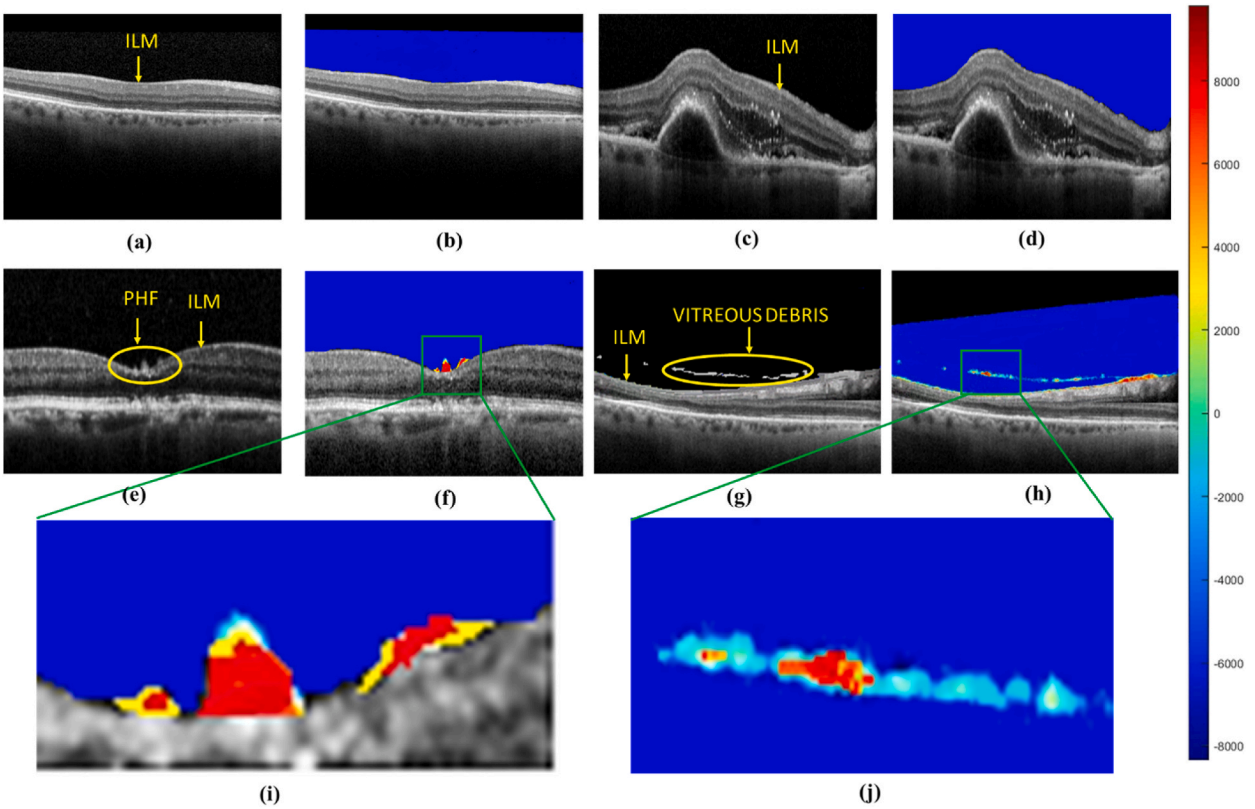

Fig. 3. Visualization of the Feature Map for the Most Discriminating Feature 'median-Laws L3S3L3' within the pre-ILM/Vitreous Compartment: (a), (c) Original Control Images; (b), (d) Feature map for 'median-Laws L3S3L3' feature for (a) and (c), respectively; (e), (g) Original Safety Images; (f), (h) Feature map for 'median-Laws L3S3L3' feature for (e) and (g), respectively. (i), (j) Zoomed-in version of (f) and (h), respectively. The PHF and vitreous debris are highly expressed as reflected by the warmer color tones of the heatmap compared to the rest of the vitreous compartment with lower feature expression (reflected by cooler color tones), PHF, Preretinal Hyperreflective Foci. (For interpretation of the references to color in this figure legend, the reader is referred to the Web version of this article.)

are 'median-Laws L3S3L3', 'skewness-Laws S3S3L3', 'median-Laws E3L3L3', 'median-Laws S3L3L3' and 'kurtosis-Gabor XY-θ = 0.000, XZ-θ = 0.000, λ = 2.668, BW = 1'. The topmost discriminating Laws energy feature 'median-Laws L3S3L3' captures the textural patterns of levels (L) in both horizontal and diagonal direction and spots (S) in vertical direction, using a 3 × 3 × 3 convolution filter. Fig. 3 (a, c, e, g) are the original images; . Fig. 3 (b, d, f, h) present the vitreous compartment feature map of Laws L3S3L3 feature for two cases of Control and Safety patients. The feature expression of the vitreous compartment is found to be low for both the Control and Safety patients. However, higher order of feature expression within the PHF (Fig. 3(f)) [zoomed-in Fig. 3(i)] and vitreous debris (Fig. 3 (h)) [zoomed-in Fig. 3(j)] is observed for the Safety patients, reflective of higher order of heterogeneity within the PHF and vitreous debris.

The box and whisker plot of the topmost two features 'median- Laws L3S3L3' and 'skewness-Laws S3S3L3' are presented in Fig. 4(a) and Fig. 4(b), respectively. Statistically significant difference between the 2 groups of patients were observed for both the features with p-value of 7.2904e-09 and 9.3253–07, respectively. The 2-D scatter plot of Control and Safety within S_{tr} is plotted in the space of the top two most discriminating texture features is presented in Fig. 4(c).

Using the most discriminating five features from F_t, M_{rf} yielded an AUC of 0.95 ± 0.03 on S_{tr} and AUC of 0.76 (95 % Confidence Interval [C·I]: 0.6, 0.85) on S_t at pre-IOI timepoint. The corresponding ACC, sensitivity and specificity values are 88 %, 76 % and 100 %, respectively. We also validated M_{rf} performance on S_t to distinguish between Control and Safety patients at the event timepoint. The corresponding AUC, ACC, sensitivity and specificity values were 0.81 (95 % Confidence Interval [C·I]:0.67, 0.9), 60 %, 60 % and 60 %, respectively.

3.3. Distinguishing control and RV/RO group based on texture-based radiomic features at pre-IOI and event timepoint

In the present study we also validated the performance of M_{rf} in discriminating the most adverse group of patients with RV/RO. M_{rf} yielded AUC of 0.74 (95 % Confidence Interval [C·I]:0.51,0.98) and ACC, sensitivity and specificity of 0.6, 0.6, and 0.7, respectively on S_t at pre-IOI time-point and AUC of 0.8 (95 % Confidence Interval [C·I]: 0.61,0.98) and ACC, sensitivity and specificity of 0.69, 0.75, and 0.7, respectively at the event time-point.

4. Discussion

Intravitreal injections of anti-vascular endothelial growth factors (anti-VEGF) are the first line of therapy for neovascular age related macular degeneration (nAMD). VEGF plays an important role in the pathogenesis of neovascularization and associated exudation [26]. Anti-VEGF agents (e.g., aflibercept, ranibizumab, bevacizumab, brolucizumab, faricimab) suppress VEGF activity and exudation and improving visual acuity (VA) in nAMD [27]. These drugs are generally well tolerated. However, a certain number of eyes develop intraocular inflammation (IOI) secondary to anti-VEGF therapy [3] and are at increased risk of VA loss. Identification of eyes at-risk for developing IOI related events could help clinicians for risk stratification of IOI at early stage.

Multiple studies have demonstrated the potential of using artificial intelligence (AI) based models to utilize OCT signatures and features for multiple valuable uses, such as monitoring disease activity and patient management, classifying AMD from OCT images and identifying biomarkers predictive of treatment response are not only sufficient. Most of the studies available in literature mainly focus on developing AI models for classification and quantification of nAMD features such as intra-retinal fluid (IRF), sub-retinal fluid (SRF), pigment epithelium detachment (PED); identifying predictive biomarkers associated with anti-VEGF therapy treatment response for nAMD and predicting disease progression using AI. The presence of IRF/intraretinal cysts (IRC) at baseline and during

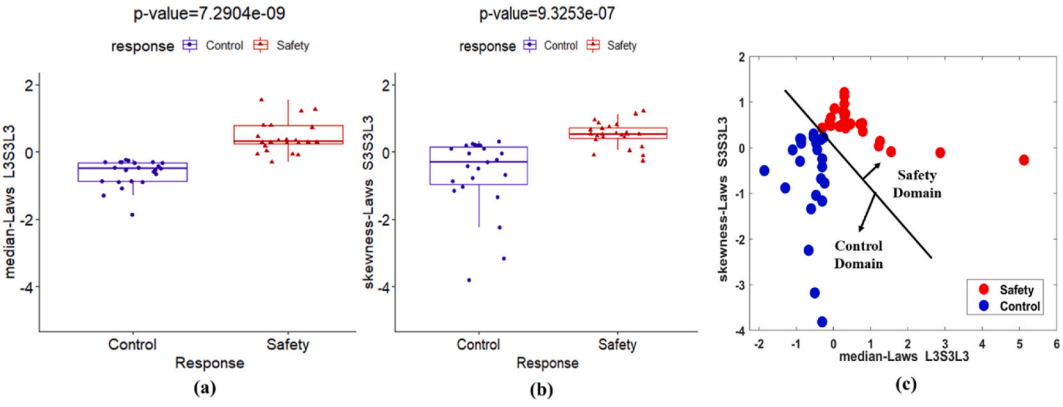

Fig. 4. *(a), (b) Box and Whisker plots showing distribution differences for the two best discriminating features between Control and Safety group. The plot on the left corresponds to the feature values for Control (N=23) and that on the right corresponds to the feature values for the Safety (N=24) group within S_{tr}. (c) A 2-D scatter plot of Control (blue dots) and Safety (red dots) within S_{tr} is plotted in the space of the top two texture features ('median- Laws L3S3L3' and 'skewness-Laws S3S3L3'). The black line was identified as the optimal linear boundary separating the Control from the Safety group within S_{tr}. S_{tr}, training set.* (For interpretation of the references to color in this figure legend, the reader is referred to the Web version of this article.)

anti-VEGF treatment regimen has been found to be associated with VA [28,29]. A significant positive correlation between SRF width and best corrected VA (BCVA) was reported by Segal et al. [30]. As reported by Casalino et al. [31], the presence of subretinal hyperreflective material (SHRM) at baseline was found to be strongly associated with poorer BCVA compared with eyes without SHRM [31]. Ehlers et al. [17] explored longitudinal assessment of retinal fluid dynamics and total retinal fluid indices in characterizing disease activity in nAMD. Based on the improvement in EZ integrity, reduction in SHRM volume, and reduction in sub-retinal pigment epithelium (RPE) disease burden over the first year of anti-VEGF treatment to nAMD eyes as reported in Ref. [32], EZ integrity measures and SHRM volume could be used as predictors of VA. Mantel et al. [33] identified certain aqueous humor molecular biomarkers that were differentially expressed between incomplete responders of anti-VEGF therapy in comparison to nAMD patients with optimal responses. All of these studies serve as an important proof of concept and are helpful in guiding future optical coherence tomography (OCT) imaging analyses, however, for monitoring disease activity and patient management, classifying AMD from OCT images and identifying biomarkers predictive of treatment response are not only sufficient. Developing AI models to identify eyes who are likely to develop adverse events such as IOI and retinal vasculitis secondary to anti-VEGF drugs in future and have increased risk of VA loss is also equally important. This would truly aid the clinicians in better monitoring of disease course and anti-VEGF drug administration process.

In the initial phase of this analysis, we identified certain texture based radiomics features characterizing heterogeneity within the vitreous compartment that best discriminated between Control and Safety group of patients. The most discriminating features were used to train a machine learning model (M_{rf}) to distinguish between the two groups of patients on the training set (S_{tr}) and validated on the independent test set (S_t). In the second phase of the study, we tested the efficacy of M_{rf} in discriminating between control and the more adverse sub-group of patients with retinal vasculitis/retinal vascular occlusion (RV/RO). Laws texture-based features were found to be differentially expressed between the patient sub-groups. Higher feature expression was observed within the vitreous debris and the pre-retinal hyper-reflective foci (PHF) for the patients from Safety group. Laws texture features capture patterns of edges, waves, ripples and spots that are most likely being reflected in the form of heterogeneity (such as abrupt changes in edges, ripples and intensity smoothness) within the texture of PHF and vitreous debris. This might be linked to the intricate textural discrepancy within the vitreous associated with the development of inflammation.

The novelty of the present work lies in the ability of the developed model (M_{rf}) to identify eyes that are most likely to develop inflammation in due course of treatment at pre-IOI timepoint, i.e., prior to the actual clinical event. In other words, even if the actual event is late, the radiomics based characterization of the vitreous compartment could identify early signal of adverse events that could help the clinicians assess underlying posterior inflammation and subsequent doses of anti-VEGF injection may be ceased. With this respect, this is very important since this could potentially help the clinicians in early stratification of IOI risk and treatment decision making.

5. Limitations of the study

The present study had limitations that must be acknowledged. The Safety Review Committee (SRC) only reviewed cases for which the investigators reported incidence of IOI, endophthalmitis, and retinal arterial occlusion; these cases tended to have more imaging available around the time of the event. However, the actual event rate may have been higher than reported by the investigators, particularly for the cases which had minimum symptom or no symptoms. This analysis was limited to treatment-naïve patients; no conclusions can be drawn relating to the incidence of these adverse events in patients with a history of anti-VEGF therapy. Further rigorous analysis of the identified biomarkers is required to explore their association with the inflammation on other datasets. Also, a detailed analysis of the sensitivity of the segmentation software needs to be addressed. Additionally, this analysis was limited to incorporating SD-OCT imaging information. The addition of multi-modal data, such as fluorescein angiography and fundus photography, might provide greater performance. However, given that SD-OCT is the gold standard imaging modality for nAMD there is a significant advantage to the simplicity of only needing that imaging modality for model performance.

6. Conclusion

In this preliminary discovery evaluation in the HAWK dataset, we investigated the role of computer-extracted OCT-derived texture-based radiomic features in discriminating the eyes with likelihood of inflammation development in nAMD. The major findings of the study are the identification of certain texture features that favorably distinguished between the Control and Safety group of patients. With further validation from multi-institutional datasets, these features could be potentially used for image characterization and early stratification of IOI risk in enhanced precision medicine for the management of nAMD patients.

Financial Support

Research reported in this publication was supported by NIH-NEI P30 Core Grant (IP30EY025585) (Cole Eye Institute), Unrestricted Grants from The Research to Prevent Blindness, Inc (Cole Eye Institute), Cleveland Eye Bank Foundation awarded to the Cole Eye Institute (Cole Eye), K23-EY022947-01A1 (JPE), the National Cancer Institute under award numbers R01CA249992, R01CA202752, R01CA208236, R01CA216579, R01CA220581, R01CA257612, R01CA268207A1, U01CA239055, U01CA248226, U54CA254566, National Heart, Lung and Blood Institute R01HL151277, R01HL158071, National Institute of Biomedical Imaging and Bioengineering R43EB028736, National Center for Research Resources under award number C06 RR12463-01, VA Merit Review Award IBX004121A

from the United States Department of Veterans Affairs Biomedical Laboratory Research and Development Service, the Office of the Assistant Secretary of Defense for Health Affairs, through the Breast Cancer Research Program (W81XWH-19-1-0668), the Prostate Cancer Research Program (W81XWH-15-1-0558, W81XWH-20-1-0851), the Lung Cancer Research Program (W81XWH-18-1-0440, W81XWH-20-1-0595), the Peer Reviewed Cancer Research Program (W81XWH-18-1-0404, W81XWH-21-1-0345), the Kidney Precision Medicine Project (KPMP) Glue Grant and sponsored research agreements from Bristol Myers-Squibb, Boehringer-Ingelheim, Eli-Lilly and Astrazeneca.

This content is solely the responsibility of the authors and does not necessarily represent the official views of the National Institutes of Health, the U.S. Department of Veterans Affairs, the Department of Defense, or the United States Government.

Standardized data reporting

Data are available upon reasonable request. Access to data sets from the Cole Eye Institute, Cleveland Clinic Foundation (used with permission for this study) should be requested directly from these institutions via their data access request forms. Subject to the institutional review boards' ethical approval, unidentified data would be made available as a test subset.

Data availability statement

The data that has been used in the present study is confidential.

CRediT authorship contribution statement

Sudeshna Sil Kar: Writing – review & editing, Writing – original draft, Methodology, Investigation, Formal analysis. **Hasan Cetin:** Writing – review & editing, Methodology, Formal analysis. **Sunil K. Srivastava:** Writing – review & editing, Conceptualization. **Anant Madabhushi:** Writing – review & editing, Supervision, Resources, Methodology, Investigation. **Justis P. Ehlers:** Writing – review & editing, Visualization, Supervision, Software, Project administration, Investigation, Funding acquisition, Conceptualization.

Declaration of competing interest

The authors declare the following financial interests/personal relationships which may be considered as potential competing interests: Justis P. Ehlers reports financial support was provided by NIH-NEI P30 Core Grant (IP30EY025585) (Cole Eye Institute). Justis P. Ehlers reports financial support was provided by Unrestricted Grants from The Research to Prevent Blindness, Inc (Cole Eye Institute). Justis P. Ehlers reports financial support was provided by Cleveland Eye Bank Foundation awarded to the Cole Eye Institute (Cole Eye), K23-EY022947-01A1 (JPE). Anant Madabhushi reports financial support was provided by the National Cancer Institute under award numbers R01CA249992, R01CA202752, R01CA208236, R01CA216579, R01CA220581, R01CA257612, R01CA268207A1, U01CA239055, U01CA248226, U54CA254566. Anant Madabhushi reports financial support was provided by National Heart, Lung and Blood Institute R01HL151277, R01HL158071. Anant Madabhushi reports financial support was provided by National Institute of Biomedical Imaging and Bioengineering R43EB028736. Anant Madabhushi reports financial support was provided by National Center for Research Resources under award number C06 RR12463-01. Anant Madabhushi reports financial support was provided by VA Merit Review Award IBX004121A from the United States Department of Veterans Affairs Biomedical Laboratory Research and Development Service. Anant Madabhushi reports financial support was provided by the Office of the Assistant Secretary of Defense for Health Affairs, through the Breast Cancer Research Program (W81XWH-19-1-0668),. Anant Madabhushi reports financial support was provided by the Office of the Assistant Secretary of Defense for Health Affairs, through Prostate Cancer Research Program (W81XWH-15-1-0558, W81XWH-20-1-0851)gh the. Anant Madabhushi reports financial support was provided by the Office of the Assistant Secretary of Defense for Health Affairs through the Lung Cancer Research Program (W81XWH-18-1-0440, W81XWH-20-1-0595). Anant Madabhushi reports financial support was provided by the Peer Reviewed Cancer Research Program (W81XWH-18-1-0404, W81XWH-21-1-0345). Anant Madabhushi reports financial support was provided by the Kidney Precision Medicine Project (KPMP) Glue Grant. Anant Madabhushi reports financial support was provided by sponsored research agreements from Bristol Myers-Squibb, Boehringer-Ingelheim, Eli-Lilly and Astrazeneca. Sunil K Srivastava reports a relationship with Regeneron that includes: consulting or advisory and funding grants. Sunil K Srivastava reports a relationship with Allergan that includes: funding grants. Sunil K Srivastava reports a relationship with Gilead that includes: funding grants. Sunil K Srivastava reports a relationship with Bausch and Lomb that includes: consulting or advisory. Sunil K Srivastava reports a relationship with Novartis that includes: consulting or advisory. Anant Madabhushi reports a relationship with Astrazeneca that includes: funding grants. Anant Madabhushi reports a relationship with Bristol Myers-Squibb that includes: funding grants. Anant Madabhushi reports a relationship with Boehringer-Ingelheim that includes: funding grants. Anant Madabhushi reports a relationship with Eli-Lilly that includes: funding grants. Anant Madabhushi reports a relationship with Picture Health Inc that includes: consulting or advisory and equity or stocks. Anant Madabhushi reports a relationship with Inspirata Inc. that includes: equity or stocks. Anant Madabhushi reports a relationship with Elucid Bioimaging that includes: equity or stocks. Anant Madabhushi reports a relationship with Aiforia that includes: consulting or advisory. Anant Madabhushi reports a relationship with Simbiosys that includes: consulting or advisory. Justis P. Ehlers reports a relationship with Aerpio that includes: funding grants. Justis P. Ehlers reports a relationship with Alcon that includes: consulting or advisory and funding grants. Justis P. Ehlers reports a relationship with Thrombogenics that includes: consulting or advisory and funding grants. Justis P. Ehlers reports a relationship with Oxurion that includes: consulting or advisory and funding grants. Justis P.

Ehlers reports a relationship with Regeneron that includes: consulting or advisory and funding grants. Justis P. Ehlers reports a relationship with Genentech that includes: consulting or advisory and funding grants. Justis P. Ehlers reports a relationship with Novartis that includes: consulting or advisory and funding grants. Justis P. Ehlers reports a relationship with Allergan that includes: consulting or advisory and funding grants. Justis P. Ehlers reports a relationship with Perceive Biotherapeutics that includes: consulting or advisory and funding grants. Justis P. Ehlers reports a relationship with Iveric Bio that includes: consulting or advisory and funding grants. Justis P. Ehlers reports a relationship with Stealth Biotherapeutics that includes: consulting or advisory and funding grants. Justis P. Ehlers reports a relationship with Roche that includes: consulting or advisory and funding grants. Justis P. Ehlers reports a relationship with Adverum that includes: consulting or advisory and funding grants. Justis P. Ehlers reports a relationship with Beyeonics that includes: consulting or advisory and funding grants. Justis P. Ehlers reports a relationship with Allegro that includes: consulting or advisory. Justis P. Ehlers reports a relationship with Leica that includes: consulting or advisory. Justis P. Ehlers reports a relationship with Zeiss that includes: consulting or advisory. Justis P. Ehlers reports a relationship with Exegenesis that includes: consulting or advisory. Justis P. Ehlers reports a relationship with Ophthalytics that includes: consulting or advisory. Justis P. Ehlers reports a relationship with BVI that includes: consulting or advisory. Anant Madabhushi has patent #United States Serial Number (USSN): 10,970,838 issued to United States. Anant Madabhushi has patent #United States Serial Number (USSN): 10,943,348 issued to United States. Justis P. Ehlers has patent issued to Leica. There is no additional Conflict of Interest If there are other authors, they declare that they have no known competing financial interests or personal relationships that could have appeared to influence the work reported in this paper.

Acknowledgement

Research reported in this publication was supported by NIH-NEI P30 Core Grant (IP30EY025585) (Cole Eye Institute), Unrestricted Grants from The Research to Prevent Blindness, Inc (Cole Eye Institute), Cleveland Eye Bank Foundation awarded to the Cole Eye Institute (Cole Eye), K23-EY022947-01A1 (JPE). Research reported in this publication was also supported by the National Cancer Institute under award numbers R01CA268287A1, U01CA269181, R01CA26820701A1, R01CA249992-01A1, R01CA202752-01A1, R01CA208236-01A1, R01CA216579-01A1, R01CA220581-01A1, R01CA257612-01A1, 1U01CA239055-01, 1U01CA248226-01, 1U54CA254566-01, National Heart, Lung and Blood Institute 1R01HL15127701A1, R01HL15807101A1, National Institute of Biomedical Imaging and Bioengineering 1R43EB028736-01, National Center for Research Resources under award number 1C06 RR12463-01, VA Merit Review Award IBX004121A from the United States Department of Veterans Affairs Biomedical Laboratory Research and Development Service the Office of the Assistant Secretary of Defense for Health Affairs, through the Breast Cancer Research Program (W81XWH-19-1-0668), the Prostate Cancer Research Program (W81XWH-20-1-0851), the Lung Cancer Research Program (W81XWH-18-1-0440, W81XWH-20-1-0595), the Peer Reviewed Cancer Research Program (W81XWH-18-1-0404, W81XWH-21-1-0345, W81XWH-21-1-0160), the Kidney Precision Medicine Project (KPMP) Glue Grant and sponsored research agreements from Bristol Myers-Squibb, Boehringer-Ingelheim, Eli-Lilly and Astrazeneca.

The content is solely the responsibility of the authors and does not necessarily represent the official views of the National Institutes of Health, the U.S. Department of Veterans Affairs, the Department of Defense, or the United States Government.

Appendix A. Supplementary data

Supplementary data to this article can be found online at https://doi.org/10.1016/j.heliyon.2024.e32232.

References

[1] H.J. Cho, M.Y. Song, W. Yoon, et al., Neovascular age-related macular degeneration in which exudation predominantly occurs as a subretinal fluid during anti-vascular endothelial growth factor treatment, Sci. Rep. 12 (2022) 3167, https://doi.org/10.1038/s41598-022-07108-4.

[2] C.S. Tan, W.K. Ngo, I.W. Chay, D.S. Ting, S.R. Sadda, Neovascular age-related macular degeneration (nAMD): a review of emerging treatment options, Clin. Ophthalmol. 16 (2022) 917–933, https://doi.org/10.2147/OPTH.S231913.

[3] J. Monés, S.K. Srivastava, G.J. Jaffe, R. Tadayoni, T.A. Albini, P.K. Kaiser, F.G. Holz, J.F. Korobelnik, I.K. Kim, C. Pruente, T.G. Murray, J.S. Heier, Risk of inflammation, retinal vasculitis, and retinal occlusion-related events with brolucizumab: post hoc review of HAWK and HARRIER, Ophthalmology 128 (7) (2021 Jul) 1050–1059, https://doi.org/10.1016/j.ophtha.2020.11.011. Epub 2020 Nov 15. PMID: 33207259.

[4] J.H. Kim, M. Sagong, S.J. Woo, et al., A real-world study assessing the impact of retinal fluid on visual acuity outcomes in patients with neovascular age-related macular degeneration in Korea, Sci. Rep. 12 (2022) 14166, https://doi.org/10.1038/s41598-022-18158-z.

[5] M.A. Zarbin, S. Francom, S. Grzeschik, et al., Systemic safety in ranibizumab-treated patients with neovascular age-related macular degeneration: a patient-level pooled analysis, Ophthalmol Retina 2 (2018) 1087e1096.

[6] S.R. Singh, M.W. Stewart, G. Chattannavar, et al., Safety of 5914 intravitreal ziv-aflibercept injections, Br. J. Ophthalmol. 103 (2019) 805e810.

[7] Bevacizumab-Ranibizumab International Trials Group, Serious AEs with bevacizumab or ranibizumab for age-related macular degeneration: meta-analysis of individual patient data, Ophthalmol Retina 1 (2017) 375e381.

[8] M.A. Hussain, A. Bhuiyan, D. Luu C, R. Theodore Smith, H. Guymer R, et al., Classification of healthy and diseased retina using SD-OCT imaging and Random Forest algorithm, PLoS One 13 (6) (2018) e0198281, https://doi.org/10.1371/journal.pone.0198281.

[9] L. Carrera-Escalé, A. Benali, A.C. Rathert, R. Martín-Pinardel, C. Bernal-Morales, A. Alé-Chilet, M. Barraso, S. Marín-Martinez, S. Feu-Basilio, J. Rosinés-Fonoll, T. Hernandez, I. Vilá, R. Castro-Dominguez, C. Oliva, I. Vinagre, E. Ortega, M. Gimenez, A. Vellido, E. Romero, J. Zarranz-Ventura, Radiomics-based assessment of OCT angiography images for diabetic retinopathy diagnosis, Ophthalmol Sci 3 (2) (2022 Nov 21) 100259, https://doi.org/10.1016/j.xops.2022.100259. PMID: 36578904; PMCID: PMC9791596.

[10] Kar S. Sil, D.D. Sevgi, V. Dong, S.K. Srivastava, A. Madabhushi, J.P. Ehlers, Multi-compartment spatially-derived radiomics from optical coherence tomography predict anti-VEGF treatment durability in macular edema secondary to retinal vascular disease: preliminary findings, IEEE J Transl Eng Health Med 9 (2021 Jul 12) 1000113, https://doi.org/10.1109/JTEHM.2021.3096378. PMID: 34350068; PMCID: PMC8328398.
[11] Sudeshna Sil Kar, Hasan Cetin, Leina Lunasco, Thuy K. Le, Robert Zahid, Xiangyi Meng, Sunil K. Srivastava, Anant Madabhushi, Justis P. Ehlers, OCT-derived radiomic features predict anti–VEGF response and durability in neovascular age-related macular degeneration, Ophthalmology Science 2 (4) (2022) 100171, https://doi.org/10.1016/j.xops.2022.100171. ISSN 2666-9145.
[12] M. Georgopoulos, K. Polak, F. Prager, et al., Characteristics of severe intraocular inflammation following intravitreal injection of bevacizumab (Avastin), Br. J. Ophthalmol. 93 (2009) 457–462.
[13] Michael Singer, Thomas A. Albini, András Seres, Caroline R. Baumal, Soumil Parikh, Richard Gale, Peter K. Kaiser, Iryna Lobach, Nicolas Feltgen, Mayur R. Joshi, Focke Ziemssen, Bahram Bodaghi, Clinical characteristics and outcomes of eyes with intraocular inflammation after brolucizumab: post hoc analysis of HAWK and HARRIER, Ophthalmology Retina 6 (2) (2022) 97–108, https://doi.org/10.1016/j.oret.2021.05.003. ISSN 2468-6530.
[14] R. Mukai, H. Matsumoto, H. Akiyama, Risk factors for emerging intraocular inflammation after intravitreal brolucizumab injection for age-related macular degeneration, PLoS One 16 (12) (2021) e0259879, https://doi.org/10.1371/journal.pone.0259879.
[15] Arrigo, Alessandro MD; Aragona, Emanuela MD; Bandello, Francesco MD, FEBO. The role of inflammation in age-related macular degeneration: updates and possible therapeutic approaches. Asia-Pacific Journal of Ophthalmology:10.1097/APO.0000000000000570, October 21, 2022. | DOI: 10.1097/APO.0000000000000570.
[16] P.U. Dugel, A. Koh, Y. Ogura, G.J. Jaffe, U. Schmidt-Erfurth, D.M. Brown, A.V. Gomes, J. Warburton, A. Weichselberger, F.G. Holz, HAWK and HARRIER Study Investigators, HAWK and HARRIER: phase 3, multicenter, randomized, double-masked trials of brolucizumab for neovascular age-related macular degeneration, Ophthalmology 127 (1) (2020 Jan) 72–84, https://doi.org/10.1016/j.ophtha.2019.04.017. Epub 2019 Apr 12. PMID: 30986442.
[17] J.P. Ehlers, J. Clark, A. Uchida, et al., Longitudinal higher-order OCT assessment of quantitative fluid dynamics and the total retinal fluid index in neovascular AMD, Trans Vis Sci Tech. 10 (29) (2021).
[18] Justis P. Ehlers, Robert Zahid, Peter K. Kaiser, Jeffrey S. Heier, David M. Brown, Xiangyi Meng, Jamie Reese, Thuy K. Le, Leina Lunasco, Ming Hu, Sunil K. Srivastava, Longitudinal assessment of ellipsoid zone integrity, subretinal hyperreflective material, and subretinal pigment epithelium disease in neovascular age-related macular degeneration, Ophthalmology Retina (2021), https://doi.org/10.1016/j.oret.2021.02.012. ISSN 2468-6530.
[19] J.P. Ehlers, A. Uchida, M. Hu, et al., Higher-order assessment of OCT in diabetic macular edema from the VISTA study: ellipsoid zone dynamics and the retinal fluid index, Ophthalmol Retina 3 (12) (2019) 1056–1066.
[20] R.M. Haralick, K. Shanmugam, I. Dinstein, Textural features for image classification, IEEE Transactions on Systems, Man, and Cybernetics SMC-3 (6) (Nov. 1973) 610–621, https://doi.org/10.1109/TSMC.1973.4309314.
[21] K.I. Laws, Textured Image Segmentation, University of Southern California Los Angeles Image Processing Inst, 1980 Jan. Report No.: USCIPI-940, http://www.dtic.mil/docs/citations/ADA083283. (Accessed 24 November 2016).
[22] A.K. Jain, F. Farrokhnia, Unsupervised texture segmentation using Gabor filters, in: 1990 IEEE International Conference on Systems, Man, and Cybernetics Conference Proceedings, Los Angeles, CA, USA, 1990, pp. 14–19, https://doi.org/10.1109/ICSMC.1990.142050.
[23] Prateek Prasanna, et al., Co-Occurrence of local anisotropic gradient orientations (CoLlAGe): a new radiomics descriptor, Sci. Rep. 6 (22 Nov) (2016) 37241, https://doi.org/10.1038/srep37241.
[24] C. Spearman, The proof and measurement of association between two things, Am. J. Psychol. 15 (1) (1904) 72, https://doi.org/10.2307/1412159.
[25] Y. Benjamini, Y. Hochberg, Controlling the false discovery rate: a practical and powerful approach to multiple testing, J. Roy. Stat. Soc. B 57 (1995) 289–300.
[26] K. Spilsbury, K.L. Garrett, W.Y. Shen, I.J. Constable, P.E. Rakoczy, Overexpression of vascular endothelial growth factor (VEGF) in the retinal pigment epithelium leads to the development of choroidal neovascularization, Am. J. Pathol. 157 (1) (2000) 135–144, https://doi.org/10.1016/S0002-9440(10)64525-7.
[27] A. Arrigo, L. Capone, R. Lattanzio, E. Aragona, P. Zollet, F. Bandello, Optical coherence tomography biomarkers of inflammation in diabetic macular edema treated by fluocinolone acetonide intravitreal drug-delivery system implant, Ophthalmol Ther 9 (4) (2020 Dec) 971–980, https://doi.org/10.1007/s40123-020-00297-z. Epub 2020 Sep 10. PMID: 32914324; PMCID: PMC7708540.
[28] D. Alex, A. Giridhar, M. Gopalakrishnan, S. Indurkhya, S. Madan, Subretinal hyperreflective material morphology in neovascular age-related macular degeneration: a case control study, Indian J. Ophthalmol. 69 (2021) 1862–1866.
[29] U. Chakravarthy, N. Pillai, A. Syntosi, L. Barclay, C. Best, A. Sagkriotis, Association between visual acuity, lesion activity markers and retreatment decisions in neovascular age-related macular degeneration, Eye 34 (2020) 2249–2256.
[30] O. Segal, E. Barayev, A.Y. Nemet, M. Mimouni, Predicting response of exudative age-related macular degeneration to Bevacizumab based on spectralis optical coherence tomography, Retina 36 (2016) 259–263.
[31] G. Casalino, A. Scialdone, F. Bandello, U. Chakravarthy, Hyperreflective material as a biomarker in neovascular age-related macular degeneration, Expet Rev. Ophthalmol. 15 (2020) 83–91.
[32] J.P. Ehlers, R. Zahid, P.K. Kaiser, J.S. Heier, D.M. Brown, X. Meng, J. Reese, T.K. Le, L. Lunasco, M. Hu, S.K. Srivastava, Longitudinal assessment of ellipsoid zone integrity, subretinal hyperreflective material, and subretinal pigment epithelium disease in neovascular age-related macular degeneration, Ophthalmol Retina 5 (12) (2021 Dec) 1204–1213, https://doi.org/10.1016/j.oret.2021.02.012. Epub 2021 Feb 26. PMID: 33640493; PMCID: PMC8387490.
[33] I. Mantel, A. Borgo, J. Guidotti, E. Forestier, O. Kirsch, Y. Derradji, P. Waridel, F. Burdet, F. Mehl, C. Schweizer, R. Roduit, Molecular biomarkers of neovascular age-related macular degeneration with incomplete response to anti-vascular endothelial growth factor treatment, Front. Pharmacol. 11 (2020) 594087, https://doi.org/10.3389/fphar.2020.594087.